Generalized Discrete Fourier Transform for FBMC Peak to Average Power Ratio Reduction

**MOHAMED A. ABOUL-DAHAB[1], (Life Senior Member, IEEE),
MOHAMED M. FOUAD[2], AND RADWA A. ROSHDY[3]**
[1]Electronics and Communications Department, Arab Academy for Science, Technology and Maritime Transport, Cairo 2033, Egypt
[2]Electronics and Communication Department, Zagazig University, Zagazig 44519, Egypt
[3]Electrical Engineering Department, Higher Technological Institute, 10th of Ramadan City 44629, Egypt

Corresponding author: Radwa A. Roshdy (radwa.roshdy@hti.edu.eg)

ABSTRACT Filter bank multicarrier (FBMC) is a strong candidate as a waveform based technique in advanced wireless communication systems (e.g. 5G), as an alternative to orthogonal frequency division multiplexing (OFDM). Like all multicarrier modulation techniques, FBMC suffers from high levels of a peak-to-average power ratio (PAPR). Discrete Fourier transform (DFT) spreading can be used in FBMC for PAPR reduction with a quite notable increase in computational complexity and without any need for side information (SI) overhead at the receiver. However, the achieved PAPR reduction is of a marginal amount, compared to the single carrier effect in the single carrier frequency division multiple access (SC-FDMA). This is due to the in-phase and quadrature phase (IQ) overlapping structure between offset quadrature amplitude modulation (OQAM) FBMC symbols. In this paper, we propose the use of generalized DFT (GDFT) spreading as an alternative to DFT spreading for PAPR reduction in systems employing FBMC. We derive the conditions at which the GDFT can totally make use of the single carrier effect of DFT spreading and hence reducing the PAPR. We also propose an enhancement algorithm that is utilized in the GDFT for further PAPR reduction without any additional complexity overhead. From the simulation results that are run at different values of subcarriers, it is shown that the GDFT spreading with the enhancement algorithm (enhanced GDFT) attain an extra amount of PAPR reduction over the other DFT spreading techniques. In addition, the GDFT spreading technique and the enhanced one also show better power spectral density (PSD) over the other DFT spreading techniques.

INDEX TERMS Filter bank multicarrier (FBMC), DFT spreading, single carrier effect, generalized DFT, PAPR reduction.

I. INTRODUCTION

Filter bank multi carrier (FBMC) technique has gainful characteristics that allow it to be a strong candidate as a waveform based technique in 5G rather than orthogonal frequency division multiplexing (OFDM) [1]–[3]. These characteristics include more robustness to frequency and synchronization misalignment [4], effective suppression in out of band (OOB) emission [5], higher bandwidth efficiency and higher data rates [6]. Nevertheless, FBMC results in high peak-to-average power ratio (PAPR) like all multicarrier modulation techniques which causes signal clipping at the receiver due

to the nonlinearity region of high power amplifier (HPA) [7]. As a result, effective suppression in out of band (OOB) emission of FBMC is still in question. In literature, there are several FBMC PAPR reduction techniques such as tone reservation (TR), in particular a sliding window TR [8], clipping and filtering [9], [10], partial transmit sequence (PTS) [11] and selected mapping (SLM) [12]. In the TR technique, a number of tones are reserved with known number of iterations and appended to the FBMC transmitted signal in a way such that the peaks of the transmitted signal are reduced. There is also a sliding window tones reservation (SW-TR) in which the peaks of the transmitted FBMC signals are reduced inside the window. However, due to the reserved tones and the required number of iterations for PAPR reduction, the loss in

The associate editor coordinating the review of this manuscript and approving it for publication was Qilian Liang.

bandwidth efficiency is about 12.5% [8]. In the clipping and filtering technique, the amplitude of the transmitted signal is reduced to a predetermined value and thus FBMC PAPR is reduced. However, signal distortion and the OOB emission are increased because of the clipping noise that cannot be totally avoided at the receiver [9], [10]. PTS and SLM have been making use of the FBMC overlapped transmitted signal to reduce PAPR based on looking for the mutually best candidates over the multiple FBMC symbols. Nevertheless, PAPR reduction has been achieved at the expense of increasing complexity and decreasing data rate because of using side information (SI) [11], [12].

A. LITERATURE REVIEW

It is obvious that the use of the previously mentioned techniques to reduce the PAPR would be on the expense of sacrificing one or more advantageous characteristics of the FBMC. Discrete Fourier Transform (DFT) spreading is considered as a PAPR reduction technique in FBMC with a quite notable increase in computational complexity and without any need for SI overhead at the receiver. This is because the DFT and its inverse (IDFT) are deterministic operations not probabilistic ones as in PTS and SLM. However, due to the in-phase and quadrature phase (IQ) overlapping structure between offset quadrature amplitude modulation (OQAM) FBMC symbols and the different pulse shaped offset quadrature amplitude modulation (OQAM) structure [6], the DFT spreading has achieved merely marginal amount of PAPR reduction compared to the single carrier frequency division multiple access (SC-FDMA) [13]–[15]. This is because DFT spreading is applied to FBMC directly just like in the SC-FDMA system. DFT spreading with a condition of an identically time shifted multicarrier (ITSM) had been proposed in [16] to totally make use of the DFT spreading single carrier effect. This condition was resolved based on phase shift pattern of the each IQ subcarrier channel. However, the amount of PAPR reduction was not so significant. An identically time shifted multicarrier (ITSM) algorithm has been proposed to maximize the amount of PAPR reduction [16]. This is done by generating four candidate signals with different PAPR and the signal with minimum PAPR was transmitted. However, this has lead to an increase in the computational complexity.

B. MOTIVATION AND CONTRIBUTIONS

The use of DFT spreading technique in FBMC systems results in a marginal reduction of PAPR. On the other hand, the DFT is characterized by the lower computational complexity. A new approach is therefore needed for reducing PAPR while keeping the computational complexity as low as possible. The generalized discrete Fourier transform (GDFT) is proposed as an alternative to the DFT in FBMC systems.

The main contributions in this paper are summarized as follows:

- The performance of using a GDFT spreading as a PAPR reduction technique in FBMC system is analyzed, and

the conditions at which the attained spreading can fully exploit the single carrier effect of the DFT are derived.
- An enhancement algorithm to enable the GDFT spreading to reduce PAPR as good as SC-FDMA is proposed without any complexity overhead. We call this technique the enhanced GDFT.
- The enhancement algorithm is applied to other DFT spreading techniques available in literature [15], [16] to compare their performance to the proposed enhanced GDFT spreading technique.
- The PAPR performance at different numbers of subcarriers is investigated for both GDFT spreading and the enhanced GDFT and compared to those other DFT spreading techniques. From the simulation results, it is shown that the GDFT spreading and the enhanced GDFT attain an extra amount of PAPR reduction over the other DFT spreading techniques.
- Power spectral density (PDS) characteristics is also investigated in order to check the performance of the proposed technique and relevant algorithms as compared to other DFT spreading techniques

The rest of the paper is organized as follows: in section II the FBMC system structure is reviewed. Section III introduces the analysis of applying GDFT to FBMC system, and the conditions by which the PAPR reduction is improved, are derived. In section IV, we propose an enhancement algorithm based on one chosen phase shift pattern from literature, and verify the outperformance of the enhanced GDFT through PAPR and PSD simulation results. In Section V, the computational complexity of the GDFT spreading techniques is analyzed, and compared to those of other DFT spreading techniques. The comparison also includes amount of PAPR reduction and the SI included. Section VI concludes the paper.

II. FBMC SYSTEM STRUCTURE

Fig. 1 shows the FBMC system structure. In this figure, we denote the number of subcarriers by M and the number of symbols by N. In FBMC according to [17], the nth complex input symbol at the mth subcarrier is denoted by $x_{m,n}$, is divided into real and imaginary components denoted by $d_{m,n}$ and $u_{m,n}$ respectively. $x_{m,n}$ is given by:

$$x_{m,n} = d_{m,n} + ju_{m,n} \qquad (1)$$

Then the real components, $d_{m,n}$ is multiplied by the phase shift pattern which is denoted by $\rho_{m,n}$ at the mth subcarrier of the upper IFFT, and imaginary components, $u_{m,n}$ is multiplied by the phase shift pattern which is denoted by $\sigma_{m,n}$ at the mth subcarrier of the lower IFFT.

In the FBMC, each subcarrier is individually applied to a real symmetric prototype filter of response $g_{m,n}(t)$. This prototype filter is characterized by what is so called the overlapping factor K, which is the ratio of the filter impulse response duration to the multicarrier symbol period T. Prototype filter with proper choice of the overlapping factor, ensures significant inter symbol interference (ISI) suppression [6].
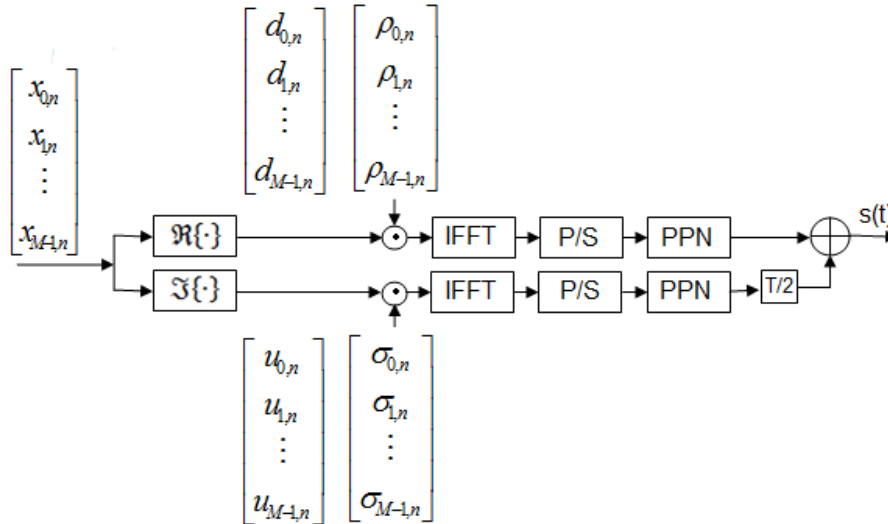
FIGURE 1. FBMC structure, ⊙ denotes element by element multiplication.

On the other hand, the use of the prototype filter results in frequency spreading, the degree of which depends upon the value of the overlapping factor K. Nevertheless, the prototype filter leads to an increase in the computational complexity [14]. The polyphase network (PPN) is found to be an effective alternative to reduce the computational complexity. This is due to the fact that it does not require frequency spreading. However, this technique inherits some additional processing [14].

Each lower and upper IFFT output vector is copied and repeated K times and then multiplied to the sampled version of the prototype filter $g_{m,n}(t)$ over K symbol duration [6]. Finally the IQ data symbols are applied to the OQAM. This OQAM ensures that the quadrature data symbols are time shifted by the half of the inverse of the subcarrier spacing. This is done by applying the output of the lower PPN to the delay block T/2, where T is the complex data symbol duration for each subcarrier as given in [6].

III. USE OF THE GENERALIZED DFT (GDFT) SPREADING IN FBMC

A. GDFT CONDITIONS FOR SINGLE CARRIER EFFECT

In this section, we derive the equations that describe the signal flow in the proposed technique, from which we can reach the conditions that are necessary to attain the single carrier effect.

If we apply the complex input symbol $x_{m,n}$ to the generalized discrete Fourier transform (GDFT) prior to the FBMC block as shown in Fig. 2, then, according to [18] the GDFT output is given by:

$$X_{m,n} = \sum_{k=0}^{M-1} x_{k,n} e^{-j(\frac{2\pi}{M})\hat{\mu}_k(m)} \tag{2}$$

where $\{\hat{\mu}_k(m)\}$ is the phase function and is given by:
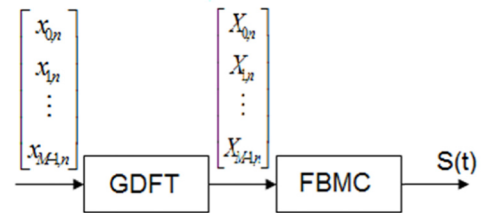
$$\hat{\mu}_k(m) = km + \psi(m) \tag{3}$$

FIGURE 2. The GDFT spreading FBMC.

where $\psi(m)$ is defined as the phase shaping function. The number of possibilities for $\psi(m) \in \mathbb{R}$ is infinite. It may be either linear or non-linear function of time, and is based on the design requirements. This function is the controlling factor that allows the FBMC to fully exploit the single carrier effect and hence reduces the PAPR. Thus throughout analysis in utilizing GDFT spreading in FBMC, the phase shaping function is used as it is. It is quite obvious that $\psi(m) = 0$ in the case of DFT, and hence DFT, is considered a special case of GDFT.

The continuous FBMC transmitted signal based on the FBMC implementation is denoted by $s(t)$ as shown in Fig. 1. It is given in [7] as:

$$s(t) = \sum_{m=0}^{M-1} \sum_{n=0}^{N-1} X_{m,n} g(t - nT) e^{j\phi_{m,n}} e^{j\frac{2\pi mt}{T}} \tag{4}$$

where $X_{m,n}$ is the complex GDFT output n^{th} symbol as defined in (2), and $g(t-nT)$ is a prototype filter response with a length (l) which equals to KN where N is the number of OQAM symbols per each subcarrier. The term $e^{j\phi_{m,n}}$ is the phase shift pattern where, $\Phi_{m,n} = \Phi_0 + \Pi/2(m + n)$. This phase shift pattern contains the real and imaginary components $\rho_{m,n}$ and $\sigma_{m,n}$ respectively. Then we can re-write (4)

according to the FBMC structure in Fig. 1 as follows:

$$s(t) = \sum_{m=0}^{M-1}\sum_{n=0}^{N-1} \Re\{X_{m,n}\}g(t-nT)\rho_{m,n}e^{j\frac{2\pi mt}{T}}$$
$$+ \Im\{X_{m,n}\}g(t-nT-\frac{T}{2})\sigma_{m,n}e^{j\frac{2\pi m}{T}(t-\frac{T}{2})} \quad (5)$$

There are many phase shift patterns in literature as given in [15], [19], [20]. However, no matter the patterns are, as long as they meet the following conditions:

$$\rho_{m,n} = \begin{cases} 1(or-1) & m = even \\ j(or-j) & n = odd \end{cases}$$

$$\sigma_{m,n} = \begin{cases} j(or-j) & m = even \\ 1(or-1) & n = odd \end{cases} \quad (6)$$

As in (1), $X_{m,n} = D_{m,n} + jU\ m,n$ where $D_{m,n}$ and $U_{m,n}$ are the real and imaginary input symbols after passing through GDFT respectively. Thus, $D_{m,n}$ and $U_{m,n}$ are given by:

$$D_{m,n} = \Re\{X_{m,n}\} = \sum_{k=0}^{M-1} d_{k,n}e^{-j\frac{2\pi}{M}(km+\psi(m))} \quad (7)$$

$$U_{m,n} = \Im\{X_{m,n}\} = \sum_{k=0}^{M-1} u_{k,n}e^{-j\frac{2\pi}{M}(km+\psi(m))} \quad (8)$$

Equation (5) may be further re-written as:

$$s(t)$$
$$= \sum_{m=0}^{M-1}\sum_{n=0}^{N-1}\sum_{k=0}^{M-1}[d_{k,n}\rho_{m,n}e^{-j\frac{2\pi}{M}(km+\psi(m))}g(t-nT)e^{j\frac{2\pi mt}{T}}]$$
$$+ [u_{k,n}\sigma_{m,n}e^{-j\frac{2\pi}{N}(k+\psi(m))}g(t-nT-\frac{T}{2})e^{j\frac{2\pi m}{T}(t-\frac{T}{2})}] \quad (9)$$

To simplify analysis, we assume that the prototype filter response $g(t)$ has a unity rectangular pulse shaping. Then for the overlapped interval of the IQ components of the nth OQAM in which $nT+T/2\le t \le (n+1)T$, then (9) can take the form:

$$s(t) = \sum_{k=0}^{M-1} d_{k,n}\sum_{m=0}^{M-1}\rho_{m,n}e^{j\frac{2\pi m}{T}(t-\frac{T}{M}(k+\frac{\psi(m)}{m}))}$$
$$+ (-1)^m\sum_{k=0}^{M-1} u_{k,n}\sum_{m=0}^{M-1}\sigma_{m,n}e^{j\frac{2\pi m}{T}(t-\frac{T}{M}(k+\frac{\psi(m)}{m}))} \quad (10)$$

Using the concept of the Dirichlet Since pulse given in [21] as $z(t) = \sum_{m=0}^{M-1} e^{j\frac{2\pi mt}{T}}$, then (10) could be re-written in the form:

$$s(t) = \sum_{k=0}^{M-1}\{d_{k,n}\rho_{m,n} + (-1)^m u_{k,n}\sigma_{m,n}\}$$
$$\times z(t-\frac{T}{M}k)z(-\frac{T\psi(m)}{Mm}) \quad (11)$$

Substituting with the phase shift pattern $\rho_{m,n} = e^{j\phi_{m,2n}}$ and $\sigma_{m,n} = e^{j\phi_{m,2n+1}}$ into (11), gives $s(t)$ as:

$$s(t) = \sum_{k=0}^{M-1}(-1)^n\{d_{k,n} + j(-1)^m u_{k,n}\}$$
$$\times z(t-\frac{T}{M}k+\frac{T}{4})z(-\frac{T\psi(m)}{Mm}) \quad (12)$$

The symbol index (k) on the FBMC subcarrier index influences the shift of the pulse $z(t-\frac{T}{M}k)$ as in (12), so in general, $z(t-\frac{T}{M}k+\frac{T}{4})$ is a shifted version of the narrow baseband pulse. In the case of canceling the term $(-1)^m$ ahead of the quadrature phase component $\{u_{k,n}\}$, then (12) will represent the single carrier signal, in which T/M spaced symbols are transmitted. To cancel it out, we set the phase shaping function $\{\psi(m)\}$ so that $z(-\frac{T\psi(m)}{Mm})$ equals to $(-1)^m$. This is achieved when $\psi(m) = mM/2$. However, the term $(-1)^m$ is canceled out from the quadrature channel component $\{u_{k,n}\}$, and appears in the phase channel component $\{d_{k,n}\}$, which means that the problem still exists. In conventional DFT spreading utilizing FBMC as in [13]–[15], the term $(-1)^m$ wasn't cancelled and hence a marginal PAPR reduction is achieved. In [16], the authors multiplied the phase shift pattern of the quadrature data symbol $\{\sigma_{m,n}\}$ by the shift term $(-1)^m$. As a result, the multicarrier for the IQ components appear identically time shifted (ITSM) [16]. However, the corresponding amount of the reduced PAPR is limited to 0.6 dB to 0.8 dB because of the overlapping interval between the IQ channels of the OQAM symbols.

In order to fully exploit the single carrier effect of DFT spreading using GDFT, there are three conditions that need to be satisfied. The first one is that the function $\psi(m)$ must be set to zero in the case of the in-phase channel component $\{d_{k,n}\}$ and set to mM/2 in the case of the quadrature channel component $\{u_{k,n}\}$. Thus (12) takes the following form:

$$s(t) = \sum_{k=0}^{M-1}(-1)^n\{d_{k,n} + ju_{k,n}\}z(t-\frac{T}{M}k+\frac{T}{4})$$
$$s(t) = (-1)^n\sum_{k=0}^{M-1}\{x_{k,n}\}z(t-\frac{T}{M}k+\frac{T}{4}) \quad (13)$$

Equation (13) represents the DFT spreading of the complex input symbol $x_{m.n}$, where $(-1)^n$ and the time shift term $T/4$ exist because of using the phase shift pattern. So, in order to make use of the single carrier effect of the DFT spreading using the GDFT, the real and imaginary parts of the complex input symbol must be separated before being applied to the GDFT as shown in Fig. 3, and this is the second condition. Either setting the phase shaping function to zero in case of in-phase channel or to mM/2 in case of quadrature channel, this means that the GDFT spreading is with linear phase, and this is the third condition.
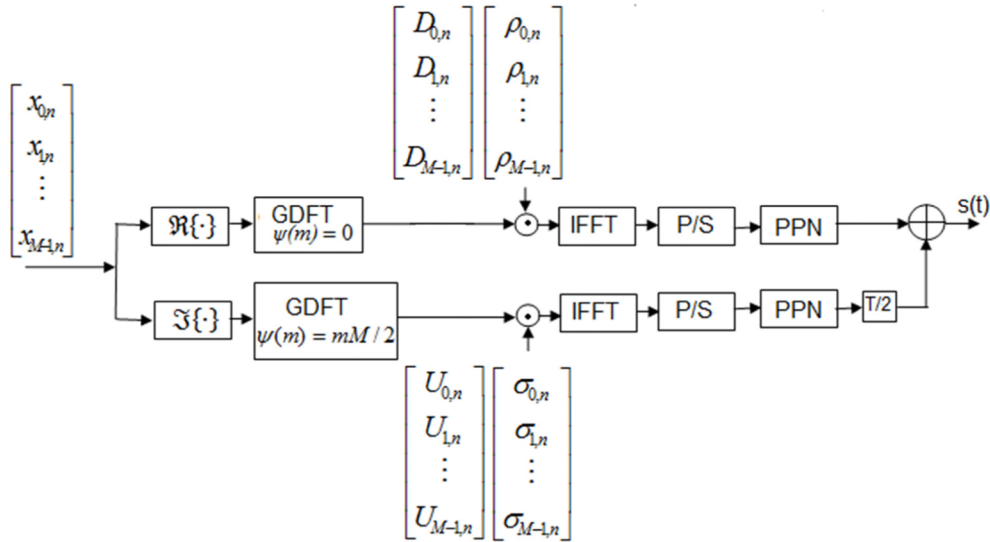
FIGURE 3. The GDFT spreading FBMC structure implementation.

B. SIMULATION RESULTS

In this sub-section we compare the PAPR performance of the GDFT spreading with that of other DFT spreading techniques, namely DFT spreading, ITSM and the improved ITSM which has been introduced in [16]. However, we shall call it the improved ITSM to remove any ambiguity in dealing with the comparative study. In addition, the original FBMC structure is included. In our analysis, the following phase shift pattern is assumed for all of the DFT spreading techniques: $\rho_{m,n} = e^{j\phi_{m,2n}}$, $\sigma_{m,n} = e^{j\phi_{m,2n+1}}$. If we use a prototype filter of response g(t) the equation (5) could be re-written as:

$$s(t) = \sum_{m=0}^{M-1} \sum_{n=0}^{N-1} (-1)^n \{D_{m,n}g(t - nT)$$

$$+ jU_{m,n}g(t - nT - \frac{T}{2})\}e^{j\frac{2\pi m}{T}(t+\frac{T}{4})} \quad (14)$$

Simulation results are carried out through developing relevant m-files using a MATLAB package. The simulation parameters used are given in table 1 below [16].

It is notable that the cross mapping of complex to real (C2R) is not used for every other subcarrier. This is because switching between IQ components implies that the phase shift pattern and the phase shaping function of ITSM and GDFT respectively must be changed correspondingly.

It is also noted from table 1 that the prototype filter used is of type PHYDAYS, of which overlapping factor is 4. This type of filters is used to facilitate comparison to other DFT spreading techniques that utilize the same filter type.

The PAPR for every symbol of FBMC is calculated as follows:

$$PAPR = \frac{\underset{(n-1)T \leq t \leq nT}{max} |s(t)|^2}{E[|s(t)|^2]} \quad n = 0, 1, \ldots, N-1 \quad (15)$$

TABLE 1. System Parameters.

Parameter	VALUE
FFT/IFFT size of FBMC	64, 128,256
Numbers of subcarriers (M)	64,128,256
Numbers of symbols/subcarriers	16
Modulation	OQPSK
Type of prototype filter	PHYDYAS filter
Overlap factor	4

where $E[|s(t)|^2]$ is the expected value of the transmitted FBMC symbols. Performance of PAPR is measured by the complementary cumulative distribution function (CCDF). It is defined as the probability that PAPR exceeds some threshold value that is denoted by (PAPR0). PAPR0 is a random variable (R.V), of which lower values indicate better performance [22].

Fig. 4 to Fig. 6 show the simulated PAPR's CCDF of the GDFT-spreading with DFT-spreading [15], ITSM [16], improved ITSM [16] and original FBMC signal (without DFT spreading) when offset quadrature phase shift keying (OQPSK) is used with number of subcarriers M = 64, 128 and 256 respectively. The PAPR of SC-FDMA is also included so as to be taken as a reference.

It is obvious from Fig. 4 that for a reference value of the CCDF of 10^{-3}, the GDFT spreading increases the amount of reduction of PAPR over ITSM and DFT spreads by nearly 1.1 dB and 1.7 dB respectively. More improvements are achieved with the increase of number of subcarriers as shown in Fig. 5 and Fig. 6. This is due to the splitting of real and imaginary symbol data before being applied to the GDFT spreading process. It is also shown in Fig. 4 that the improved ITSM results in more PAPR reduction over the GDFT spreading by nearly 0.7 dB. However, the value of this reduction
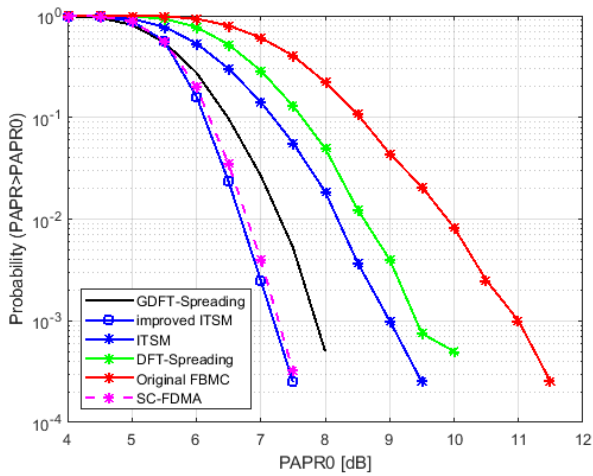
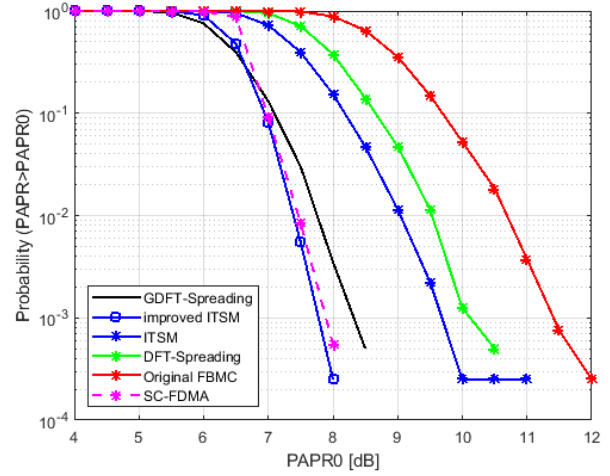**FIGURE 4.** PAPR's CCDF of different FBMC DFT spreading techniques M = 64.

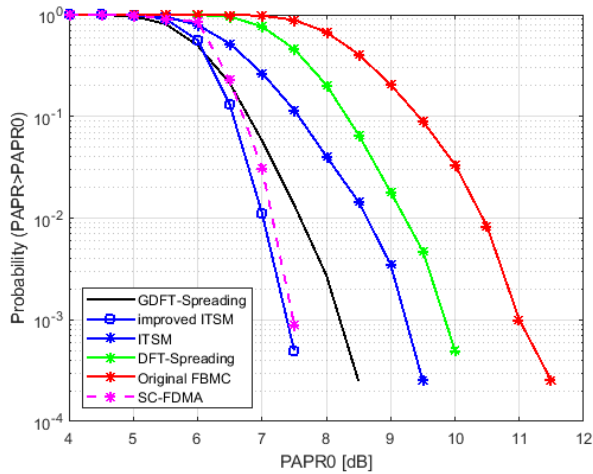**FIGURE 5.** PAPR's CCDF of different FBMC DFT spreading techniques M = 128.

FIGURE 6. PAPR's CCDF of different FBMC DFT spreading techniques M = 256.
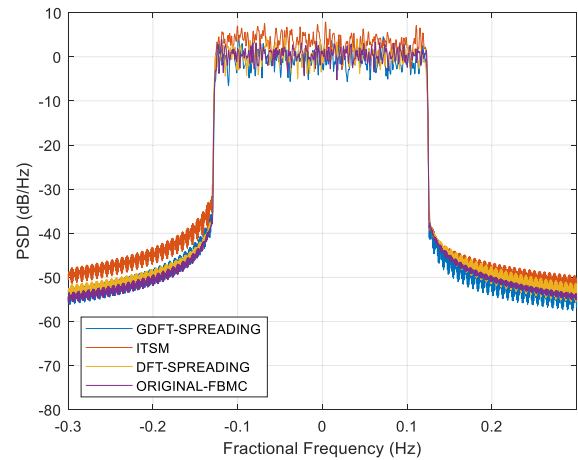

FIGURE 7. PSD of different DFT spreading techniques with M = 64.

becomes lower as the number of subcarrier increases as shown in Fig. 5 and Fig. 6. The reason is that the improved ITSM inherits some modification in FBMC structure with a complexity and SI overhead to achieve this result. The modification implies using four waveform candidates with different PAPR and transmitting the one with minimum value.

The simulated power spectral density (PSD) of the GDFT spreading versus ITSM, DFT spreading and original FBMC are illustrated in Fig. 7. Compared to ITSM and DFT spreading, the GDFT spreading has lower out-of-band (OOB) emission by −3 dB, −2 dB respectively when a fractional frequency offset of 0.2 Hz is considered. It is clear from this figure that using GDFT in FBMC PAPR reduction doesn't affect the PSD. It remains nearly unchanged compared to the PSD of original FBMC. It is worth mentioning that the improved ITSM is not included in the simulated PSD and BER results as it has the same PSD and BER as that of the ITSM.

IV. A PROPOSED ENHANCED GDFT ALGORITHM

It is obvious from Fig. 4 to Fig. 6 that the PAPR reduction performance of the improved ITSM is better than that of the GDFT spreading, nearly about 0.6 dB. So here, we propose the enhancement GDFT algorithm to boost the PAPR reduction of the GDFT spreading.

From (14), it is noted that the quadrature channel is delayed by T/2 for OQAM before multicarrier modulation. If the In-phase channel is delayed by T/2, then the conditions of phase shaping functions that are derived in section (III-A) are still valid. However, the delayed in-phase signal and delayed quadrature one have different PAPR's. This is because, as illustrated in [16], the delayed channel symbol overlaps the incoming OQAM symbol and the non-delayed channel symbol overlaps the previous symbol. Consequently, the parts of the signal outside the overlapped interval are different depending on which channel is delayed and thus, the PAPR's of the two signals are different. If the In-phase
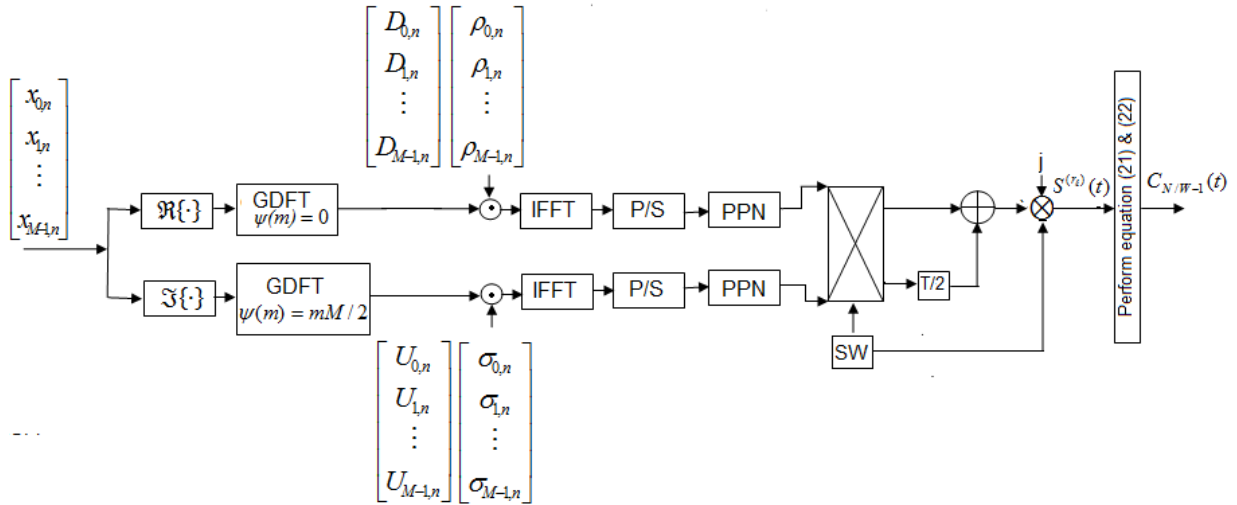
FIGURE 8. The structure of enhanced GDFT spreading.

channel is delayed by T/2, then (14) will be:

$$s(t) = \sum_{m=0}^{M-1} \sum_{n=0}^{N-1} (-1)^n \{ D_{m,n} g(t - nT - \frac{T}{2})$$
$$+ j U_{m,n} g(t - nT) \} e^{j\frac{2\pi m}{T}(t + \frac{T}{4})} \quad (16)$$

In this case, we have two distinct candidate GDFT signals with different peak powers. The proposed enhancement algorithm compares the PAPR of the two signals with each other and the one with the minimum PAPR is selected and transmitted. The main idea behind proposing this algorithm is applying one half symbol delayed for both the in-phase and quadrature channels. It is noticed from (14) and (16) that the operator (j) is multiplied by the delayed and previous channels respectively. This is done in order that the successive data blocks for the selected signal could be added. To maintain the FBMC signal format unchanged the operator (j) must be multiplied by the RHS of (16). This is done by using a switch after the PPN as shown in Fig. 8. The proposed enhancement algorithm is accomplished through the following steps:

Step 1: Divide the data frame into a successive number of (*l*) blocks, each block contains a number of symbols equals to W.

Step 2: The symbol index (*n*) is limited to the (*ℓth*) data block such that $\ell W \leq n \leq (\ell + 1)W + 1$. When the switch (SW) is ON the first candidate signal is generated for every (*ℓth*) data block as follows:

$$s(t)_\ell^{(1)} = \sum_{m=0}^{M-1} \sum_{n=\ell W}^{(\ell+1)W-1} (-1)^n \{ D_{m,n} g(t - nT)$$
$$+ j U_{m,n} g(t - nT - \frac{T}{2}) \} e^{j\frac{2\pi m}{T}(t + \frac{T}{4})} \quad (17)$$

When (SW) is OFF the second candidate signal is generated for every (*ℓth*) data block as follows:

$$s(t)_\ell^{(2)} = \sum_{m=0}^{M-1} \sum_{n=\ell W}^{(\ell+1)W-1} (-1)^n \{ j D_{m,n} g(t - nT - \frac{T}{2})$$
$$- U_{m,n} g(t - nT) \} e^{j\frac{2\pi m}{T}(t + \frac{T}{4})} \quad (18)$$

Step 3: The PAPR of the two signals are calculated every data block, and the signal with the minimum PAPR is selected and concatenated with the selected signal achieving minimum PAPR in the next data blocks.

Let $C_\ell(t)$ to be the concatenated signal up to (*ℓth*) block. It is defined as:

$$C_\ell(t) = s^{(r_\ell)}(t) \quad (19)$$

where (r_ℓ) is the index of the selected candidate signal. For the first block ($\ell = 0$) it is calculated as:

$$r_\ell = \arg\min_{a \in \{1,2\}} \{ \max_{\ell \in R} \left| s_\ell^{(a)}(t) \right|^2 \} \quad (20)$$

where R denotes the search zone of the peak power, and it is limited to the present data block signal $s_\ell^{(a)}(t)$, where it is set to $[\ell WT - \frac{rT}{2}, (\ell + 1)WT + \frac{T}{2} + \frac{KT}{2}]$.

For ($\ell \geq 1$), the peak power is calculated for:

$$C_\ell(t) = C_{\ell-1}(t) + s_\ell^{(a)}(t) \quad (21)$$

The signals $C_{\ell-1}(t)$ and $s_\ell^{(a)}(t)$ overlap because of the pulse shaping and the OQAM IQ staggering. The index of the selected candidate signal is defined as follows:

$$r_\ell = \arg\min_{a \in \{1,2\}} \{ \max_{\ell \in R} \left| C_{\ell-1}(t) + s_\ell^{(a)}(t) \right|^2 \} \quad (22)$$

At the end of the data blocks, the signal with minimum PAPR is selected and transmitted.

The FBMC structure that employs the enhancement GDFT algorithm is shown in Fig. 8. We shall call the

Algorithm 1 The Enhanced GDFT Spreading

Initialization
$\ell_{=16}$
W = 1
Process
FOR i = 0:ℓ
FOR ii = 1:W
Calculate $S_i^1(t)$ in equation (17)
Calculate $S_i^2(t)$ in equation (18)
END
PAPR1(i) = $\dfrac{\max\{|s_i^1(t)|^2\}}{E[|s_i^1(t)|^2]}$

PAPR2(i) = $\dfrac{\max\{|s_i^2(t)|^2\}}{E[|s_i^2(t)|^2]}$
IFPAPR1(i) < PAPR2(i)
The selected signal is $S_i^1(t)$
ELSEIFPAPR2(i) < PAPR1(i)
The selected signal is $S_i^2(t)$
END
Calculate equation (21)
END

GDFT spreading technique that utilizes the enhancement algorithm, the ''enhanced GDFT''. It is important to highlight the fact that the enhanced GDFT spreading (Fig.8) still has the same structure as that of the GDFT (Fig.3).

A. SIMULATION RESULTS

To investigate the effectiveness of the GDFT spreading technique with the relevant proposed algorithm (enhanced GDFT), its performance is compared to other similar techniques while utilizing the proposed algorithm. Simulation results are carried out through developing relevant m-files using MATLAB package. The simulation parameters used are given in table 1. The simulation results of the PAPR's CCDF are shown in Fig. 9 to Fig. 11 when utilizing OQPSK with different number of subcarriers M = 64, M = 128 and M = 256. It is clear from the simulated results that the performance of the enhanced GDFT spreading technique approaches that of the SC-FDMA in case of M = 64. At higher value of M (M = 128, 256), the performance goes better. It is also observed that the performance of the proposed enhanced GDFT spreading is superior to those of other techniques while utilizing the same proposed algorithm. This is because the two generated signals of the GDFT spreading have a PAPR value that is lower than that of the two generated signals of other techniques. It is quite notable from the results shown in Fig. 9 to Fig. 11 that at CCDF = 10^{-3}, the enhanced GDFT spreading results in a reduction of PAPR by a value of nearly 0.9 dB, 1.6 dB and 2.8 dB compared to enhanced ITSM, enhanced DFT spreading and enhanced FBMC. In the case of the GDFT spreading, the simulation results show that the PAPR reduction of the enhanced GDFT spreading is increased by 0.7 dB, 0.9 dB and 0.5 dB in the case of M = 64, 128 and 256 respectively.
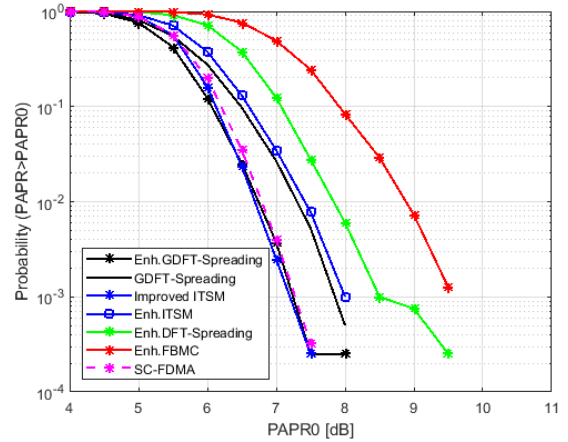

FIGURE 9. PAPR's CCDF of the enhanced GDFT spreading versus FBMC DFT spreading techniques with M = 64.
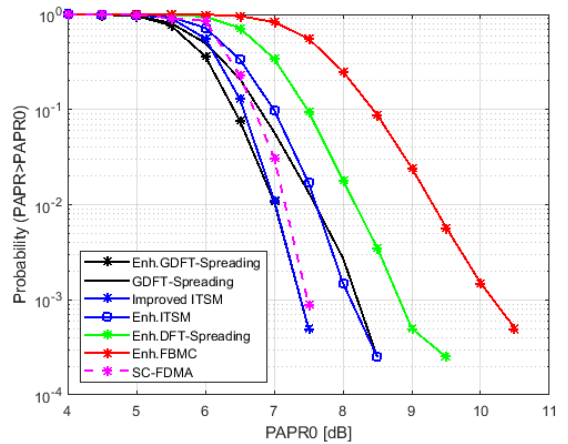

FIGURE 10. PAPR's CCDF of the enhanced GDFT spreading versus FBMC DFT spreading techniques with M = 128.

Regarding the PSD, it is clear from Fig. 12 that the enhanced GDFT algorithm has a lower OOB emission than that of the enhanced FBMC, enhanced DFT, enhanced ITSM and the proposed ITSM. Compared to the improved ITSM, the enhanced ITSM and the enhanced DFT spreading, the enhanced GDFT algorithm has lower out- of-band (OOB) emission of about −5 dB, −3 dB and −2 dB respectively when a fractional frequency of 0.2 Hz is considered.

B. COMPUTATIONAL COMPLEXITY COMPARISON

We present a comparison for computational complexity and SI between the enhanced GDFT spreading technique and the other spreading techniques, beside the probabilistic PAPR reduction techniques, namely spares PTS [23] and dispersive SLM [24]. The computational complexity in this paper is measured based on the real multiplications (RMs) only, since they carry the highest computational load.

With *M* subcarriers of power 2, the computational complexity of The GDFT is calculated as it is given in [25] and it is measured by *4x(M log₂M)*, where the number (4)

TABLE 2. comparison for different FBMC PAPR reduction techniques.

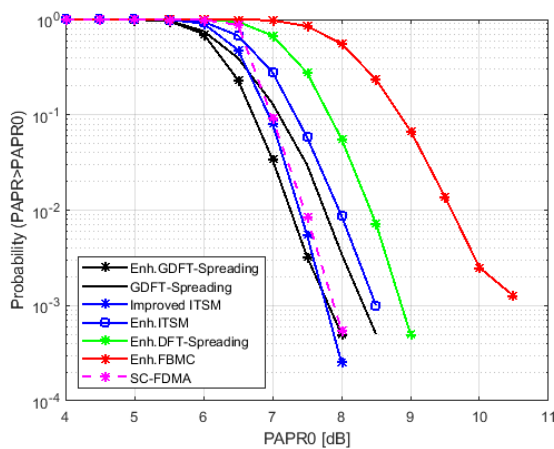| PAPR reduction Technique	Computational complexity/symbol period With M=64 and K=4			SI per data block (bits)	PAPR reduction compared to original FBMC with M=64 at CCDF=10⁻³
	Main calculations	Formula of the Real Multiplication (RM)	Order of the RMs		
Original FBMC[28]	2 IFFTs and 2 PPNs	IFFT: $4 \times (2M \log_2 M + 2M)$ PPN: $8KM$	11264	0	0 dB
DFT spreading[15]	1 DFT, 2 IFFTs and 2PPNs	DFT: $4 \times (M/2 \log_2 M)$ IFFT: $4 \times (2M \log_2 M + 2M)$ PPN: $8KM$	12032	0	1 dB
ITSM[16]	1 DFT, 2 IFFTs and 2PPNs		12032	0	1.9 dB
The improved ITSM[16]	1 DFT, 2 IFFTs and 4 PPNs		18176	2 bits	3.7 dB
GDFT spreading	1 DFT, 1 GDFT,2 IFFTs and 2 PPNs	GDFT: $4 \times (M \log_2 M)$ DFT: $4 \times (M/2 \log_2 M)$ IFFT: $4 \times (2M \log_2 M + 2M)$ PPN: $8KM$	13568	0	3.1 dB
The enhanced GDFT spreading	1 DFT, 1 GDFT,2 IFFTs and 2 PPNs		13568	1 bit	3.7 dB
Sparse PTS, V(No. of portion)=4, I(No. of iterations)=6[23]	2V IFFT, IV(2ᵛ+1) RMs and 2 PPNs	$16VM \log_2 M + 16KM + IV (2^V + 1)$	31128	IV/N	3.2 dB
Dispersive SLM, U (No. of candidates transmitted signals)=8[24]	2 U IFFT, UM RMs and 2 UPPNs	$16UM \log_2 M + 16KUM + 26 UN$	90624	Nlog₂U/N	2.3 dB

FIGURE 11. PAPR's CCDF of the enhanced GDFT spreading versus FBMC DFT spreading techniques with M = 256.

FIGURE 12. PSD of different enhanced DFT spreading techniques with M = 64.

indicates the number of RMs per one complex multiplication. The computational complexity of M-point IFFT with M subcarriers of power 2 is given by $4 \times (M \log_2 M + 2M)$ [26], and the computational complexity of DFT with M subcarriers of power 2 is given by $4 \times (M/2) \log_2 M$ respectively [27]. The number of RMs of the PPN is given by $8KM$ [28]. The computational complexity of the PTS according to [23] is given by $16VM \log_2 M + 16KM + IV (2^V + 1)$ where V and I are the number of portions and the number of iterations in spares PTS respectively. The computational complexity of the dispersive SLM according to [24] is given by $16UM \log_2 M + 16KUM + 26 UN$ where U is the number of candidates transmitted signals. The computational complexity of the improved ITSM according to [16] is given by $18 M \log_2 M + 32KM + 48M$.
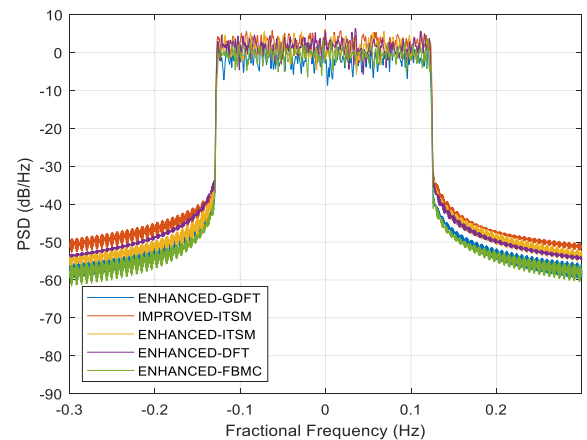
Table 2 illustrates a comparison of the computational complexities of the proposed enhanced GDFT spreading technique and the other spreading ones. The table also includes the PAPR reduction as well as the SI overhead in order to evaluate the performance of the proposed enhanced GDFT spreading. We include the sparse PTS and dispersive SLM techniques that are in given [23] and [24] since they are the most usable techniques for FBMC PAPR reduction with reduced computational complexity. It is depicted from table 2 that using GDFT spreading reduces the PAPR with complexity overhead more than those of DFT spreading and ITSM, but still the complexity overhead is lower than that of the improved ITSM, PTS and SLM. It is also obvious that the use of the proposed enhanced GDFT spreading boosts the amount of PAPR reduction better than the GDFT spreading with the same computational complexity. It is clear from table 2 that the enhanced GDFT gives nearly the same PAPR reduction

value as that of the improved ITSM, for M = 64. However, the computational complexity of the proposed enhanced GDFT is lower than that of the improved ITSM. The enhanced GDFT requires only one bit SI per data block as the algorithm is based on generating two distinct signals with different PAPR. In the case of the improved ITSM algorithm, the required SI bits per data block are two bits as its algorithm is based on generating four distinct signals with different PAPR's. This comparison shows that the enhanced GDFT combines the advantages of higher PAPR reduction, lower computational complexity and lower SI among other techniques.

V. CONCLUSION
A Generalized Discrete Fourier Transform (GDFT) was proposed to improve the PAPR performance in communication systems utilizing FBMC techniques. From the simulation results, it was shown that the use of the GDFT results in a significant reduction of PAPR. In addition, an enhanced algorithm was proposed to allow further reduction of PAPR. The performance of the enhanced GDFT was investigated versus other spreading techniques, namely DFT, ITSM, the improved ITSM and original FBMC. The simulation results showed that the proposed enhanced GDFT yields an optimum compromise between PAPR reduction value, lower OOB emission, lower SI bits and the lower degree of computational complexity among other spreading techniques. This approach would be much more suitable for meeting 5G requirements.

REFERENCES
[1] R. Gerzaguet, N. Bartzoudis, L. G. Baltar, V. Berg, J.-B. Doné, D. Kténas, O. Font-Bach, X. Mestre, M. Payaró, M. Färber, and K. Roth, "The 5G candidate waveform race: A comparison of complexity and performance," *EURASIP J. Wireless Commun. Netw.*, vol. 2017, pp. 13–26, Jan. 2017.

[2] *IMT Vision—Framework and Overall Objectives of the Future Development of IMT for 2020 and Beyond*, document ITU-R Rec M.2083-0, Sep. 2015.

[3] B. Farhang-Boroujeny, "Filter bank multicarrier modulation: A waveform candidate for 5g and beyond," *Adv. Electr. Eng.*, vol. 2014, Nov. 2014, Art. no. 482805.

[4] R. Chávez-Santiago, M. Szydełko, A. Kliks, F. Foukalas, Y. Haggad, K. E. Nolan, M. Y. Kelly, M. T. Masonta, and I. Balasingham, "5G: The convergence of wireless communications," *Wireless Pers. Commun.*, vol. 83, no. 3, pp. 1617–1642, Aug. 2015.

[5] R. Zakaria and D. Le Ruyet, "Theoretical analysis of the power spectral density for FFT-FBMC signals," *IEEE Commun. Lett.*, vol. 20, no. 9, pp. 1748–1751, Sep. 2016.

[6] G. B. Doré, R. Gerzaguet, N. Cassiau, and D. Ktenas, "Waveform contenders for 5G: Description, analysis and comparison," *Phys. Commun.*, vol. 24, pp. 46–61, Sep. 2017.

[7] H. Wang, X. Wang, L. Xu, and W. Du, "Hybrid PAPR reduction scheme for FBMC/OQAM systems based on multi data block PTS and TR methods," *IEEE Access*, vol. 4, pp. 4761–4768, 2016.

[8] S. Lu, D. Qu, and Y. He, "Sliding window tone reservation technique for the peak-to-average power ratio reduction of FBMC-OQAM signals," *IEEE Wireless Commun. Lett.*, vol. 1, no. 4, pp. 268–271, Aug. 2012.

[9] Z. Kollár and P. Horváth, "PAPR reduction of FBMC by clipping and its iterative compensation," *J. Comput. Netw. Commun.*, vol. 2012, no. 1, Feb. 201, Art. no. 382736.

[10] Z. Kollar, L. Varga, and K. Czimer, "Clipping-based iterative PAPR-reduction techniques for FBMC," in *Proc. 17th Int. OFDM Workshop (InOWo)*, Essen, Germany, Aug. 2012, pp. 1–12.

[11] C. Ye, Z. Li, T. Jiang, C. Ni, and Q. Qi, "PAPR reduction of OQAM-OFDM signals using segmental PTS scheme with low complexity," *IEEE Trans. Broadcast.*, vol. 60, no. 1, pp. 141–147, Mar. 2013.

[12] N. Shi and S. Wei, "A partial transmit sequences based approach for the reduction of peak-to-average power ratio in FBMC system," in *Proc. 25th Wireless Opt. Commun. Conf. (WOCC)*, Chengdu, China, May 2016, pp. 1–3.

[13] A. Viholainen, M. Bellanger, and M. Huchard. (2009). *PHYDAS-PHYsical Layer for Dynamic Access and Cognitive Radio Report D5.1.* [Online]. Available: www.ict-phydyas.org/delivrables/PHYDAS-D5-1.pdf

[14] C. H. Yuen, P. Amini, and B. Farhang-Boroujeny, "Single carrier frequency division multiple access (SC-FDMA) for filter bank multicarrier communication systems," in *Proc. the 5th Int. Conf. Cogn. Radio Oriented Wireless Netw. Commun.*, Cannes, France, Jun. 2010, pp. 1–5.

[15] T. Ihalainen, A. Viholainen, T. H. Stitz, M. Renfors, and M. Bellanger, "Filter bank based multi-mode multiple access scheme for wireless uplink," in *Proc. 17th Eur. Signal Process. Conf. (EUSIPCO)*, Glasgow, U.K., vol. 9, Aug. 2009, pp. 1354–1358.

[16] D. Na and K. Choi, "Low PAPR FBMC," *IEEE Trans. Wireless Commun.*, vol. 17, no. 1, pp. 182–193, Jan. 2018.

[17] B. Farhang-Boroujeny, "Filter bank multicarrier modulation: A waveform candidate for 5G and beyond," *Adv. Elect. Eng.*, vol. 2014, Dec. 2014, Art. no. 482805.

[18] A. N. Akansu and H. Agirman-Tosun, "Generalized discrete Fourier transform with nonlinear phase," *IEEE Trans. Signal Process.*, vol. 58, no. 9, pp. 4547–4556, Sep. 2010.

[19] T. Ihalainen, A. Ikhlef, J. Louveaux, and M. Renfors, "Channel equalization for multi-antenna FBMC/OQAM receivers," *IEEE Trans. Veh. Technol.*, vol. 60, no. 5, pp. 2070–2085, Jun. 2011.

[20] Z. Kollár, L. Varga, B. Horváth, P. Bakki, and J. Bitó, "Evaluation of clipping based iterative PAPR reduction techniques for FBMC systems," *Sci. World J.*, vol. 2014, Jan. 2014, Art. no. 841680.

[21] M. Amiri and V. Prenosil, "The discrete Fourier transform," in *Understanding Digital Signal Processing*, 3rd ed. New York, NY, USA: Richard lyons, 2011, pp. 74–128.

[22] M. A. AboulDahab, M. M. Fouad, and R. A. Roshdy, "A proposed preamble based channel estimation method for FBMC in 5G wireless channels," in *Proc. 35th Nat. Radio Sci. Conf. (NRSC)*, Cairo, Egypt, Mar. 2018, pp. 140–148.

[23] S. Ren, H. Deng, X. Qian, and Y. Liu, "Sparse PTS scheme based on TR schemes for PAPR reduction in FBMC-OQAM systems," *IET Commun.*, vol. 12, no. 14, pp. 1722–1727, Aug. 2018.

[24] S. S. K. C. Bulusu, H. Shaiek, D. Roviras, and R. Zayani, "Reduction of PAPR for FBMC-OQAM systems using dispersive SLM technique," in *Proc. 11th Int. Symp. Wireless Commun. Syst. (ISWCS)*, Aug. 2014, pp. 568–572.

[25] S. Weiß, M. Harteneck, and R. Stewart, "Design and efficient implementation of oversampled GDFT filter banks for subband adaptive filtering," in *Proc. IEE Colloq. Digit. Filters, Enabling Technol. Dig.*, May 2000, pp. 1–7.

[26] . Z. Kollár and H. Al-Amaireh, "FBMC transmitters with reduced complexity," *Radioengineering*, vol. 27, no. 4, pp. 1147–1154, Dec. 2018.

[27] C.-L. Wang and Y. Ouyang, "Low-complexity selected mapping schemes for peak-to-average power ratio reduction in OFDM systems," *IEEE Trans. Signal Process.*, vol. 53, no. 12, pp. 4652–4660, Dec. 2005.

[28] M. Bellanger, D. L. Ruyet, D. Roviras, and M. Terre, *FBMC Physical Layer: A Primer*, document PHYDAS FP7, Jan. 2010.

MOHAMED A. ABOUL-DAHAB (LSM'18) received the B.Sc. degree in communication engineering from the Faculty of Engineering, Cairo University, in 1973, and the M.Sc. and Ph.D. degrees in communication engineering from Alexandria University, Egypt, in 1980 and 1986, respectively. He has been a Professor of communications engineering with the Arab Academy for Science, Technology and Maritime Transport, Egypt, since 1999. He was the former Head of the Electronics and Computer Engineering Department, from 1995 to 2002, and the former Dean of the College of Engineering and Technology, Arab Academy for Science and Technology and Maritime Transport (AASTMT) (Cairo Campus), from 2002 to 2008. His publications are in the areas of antennas, channel coding and wireless networks, in addition to some publications in the field of education. He had been a member of the National Radio Science Committee, from 1993 to 2015, and has been the Chairman of the National Committee of the ITU, since 2015, both are belonging to the Academy of Scientific Research and Technology, Egypt.

MOHAMED M. FOUAD received the B.Sc. and M.Sc. degrees in Electronics and Communications Engineering Department, Menofia University, Menofia, Egypt, in 1978 and 1984, respectively, and the Ph.D. degree from the Electronics and Communication Engineering Department, Faculty of Engineering, Alexandria University, Alexandria, Egypt, in 1991. He is currently a Professor with the Electronics and Communications Department, Zagazig University.

He has published papers in international conferences in the areas of communications and electronics. His research interests are in digital communication systems, and mobile communication systems and satellites.

RADWA A. ROSHDY received the B.Sc. and M.Sc. degrees from the Electronics and Communications Engineering Department, Zagazig University, Zagazig, Egypt, in 2008 and 2014, respectively. She is currently an Assistant Lecturer with the Electrical and Computer Engineering Department, Higher Technological Institute, 10th of Ramadan City. Her research interests are in communication security, digital communication systems, and waveform design for next generation networks.

● ● ●